Supplementary Information

# Highly Stable and Efficient All-Inorganic Lead-Free Perovskite Solar Cells with Native-Oxide Passivation

Chen et al

# Supplementary Information

## Highly Stable and Efficient All-Inorganic Lead-Free Perovskite Solar Cells with Native-Oxide Passivation

Min Chen,[1] Ming-Gang Ju,[2] Hector F. Garces,[1] Alexander D Carl,[3] Katsuya Ono,[4] Zafer Hawash,[4] Yi Zhang,[1] Tianyi Shen,[1] Yabing Qi,[4] Ronald L. Grimm,[3] Domenico Pacifici,[1] Xiao Cheng Zeng,[2] Yuanyuan Zhou,[1,*] Nitin P. Padture[1,*]

[1] School of Engineering, Brown University, Providence, Rhode Island 02912, United States

[2] Department of Chemistry, University of Nebraska−Lincoln, Lincoln, Nebraska 68588, United States

[3] Department of Chemistry and Biochemistry, Worcester Polytechnic Institute, Worcester, MA 01609, United States

[4] Energy Materials and Surface Sciences Unit, Okinawa Institute of Science and Technology Graduate University, Okinawa 904-0495, Japan

[*]Contact: yuanyuan_zhou@brown.edu (Y.Z.); nitin_padture@brown.edu (N.P.P.);

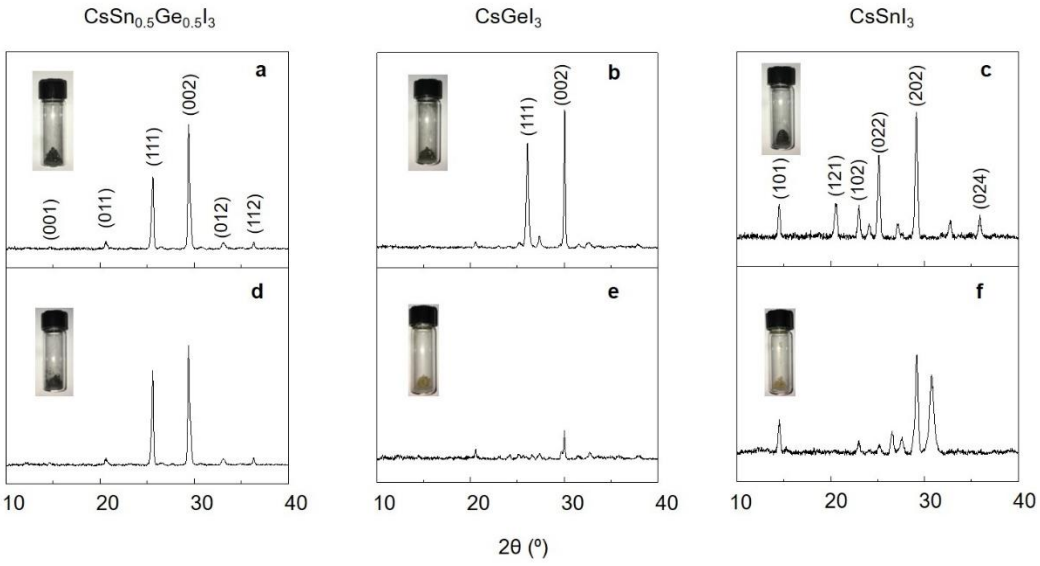


**Supplementary Figure 1. Relative stability $CsSn_{0.5}Ge_{0.5}I_3$, $CsGeI_3$ and $CsSnI_3$.** (a, b, c) XRD patterns of as-synthesized $CsSn_{0.5}Ge_{0.5}I_3$, $CsGeI_3$ and $CsSnI_3$ powders, respectively. (d, e, f) XRD patterns of $CsSn_{0.5}Ge_{0.5}I_3$, $CsGeI_3$, and $CsSnI_3$ powders after 24-h exposure to air (25 ˚C, 80% RH), respectively. Insets: photograph of the respective powders.

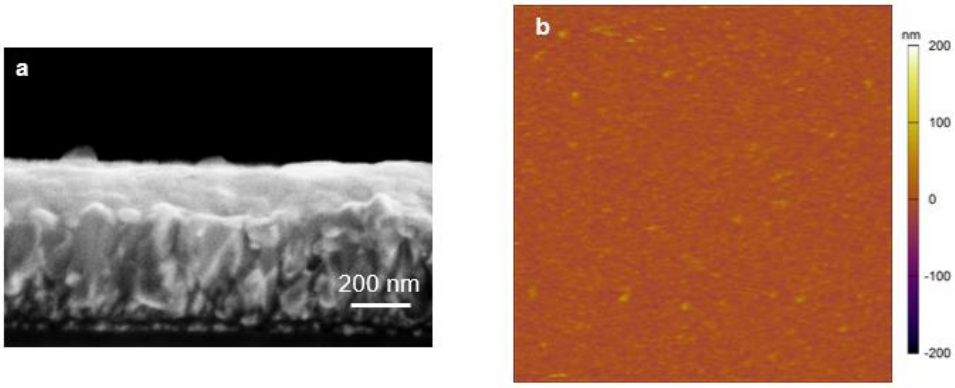


**Supplementary Figure 2. Thin film morphology characterization.** (a) Cross-sectional SEM of the $CsSn_{0.5}Ge_{0.5}I_3$ perovskite thin film. (b) Top-surface AFM image of the $CsSn_{0.5}Ge_{0.5}I_3$ perovskite thin film over a 50×50-$\mu m^2$ area.

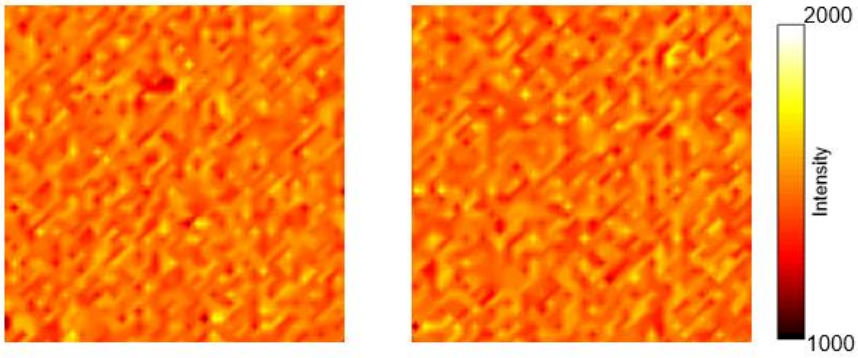


**Supplementary Figure 3. PL mapping.** PL maps over 50×50-μm$^2$ areas from two different regions in the same $CsSn_{0.5}Ge_{0.5}I_3$ perovskite thin film.

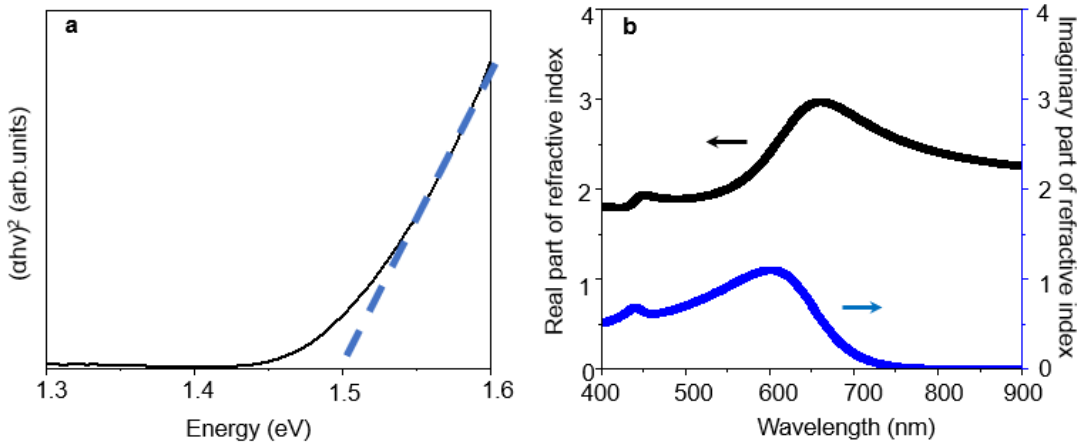


**Supplementary Figure 4. Optical characterization.** (a) Tauc plot of the $CsSn_{0.5}Ge_{0.5}I_3$ perovskite thin film. (b) Refractive index of the $CsSn_{0.5}Ge_{0.5}I_3$ perovskite thin film fitted from the ellipsometry data.

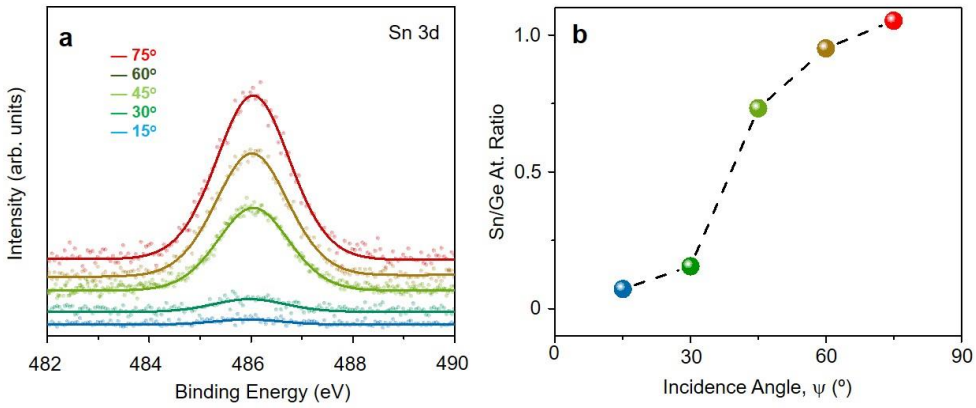


**Supplementary Figure 5. XPS characterization.** (a) Sn 3d XPS spectra, at different incidence angles, from $CsSn_{0.5}Ge_{0.5}I_3$ perovskite thin film that has been exposed to air. (b) Sn:Ge atomic ratio extracted from the Ge 3d and Sn 3d XPS data at different incidence angles.

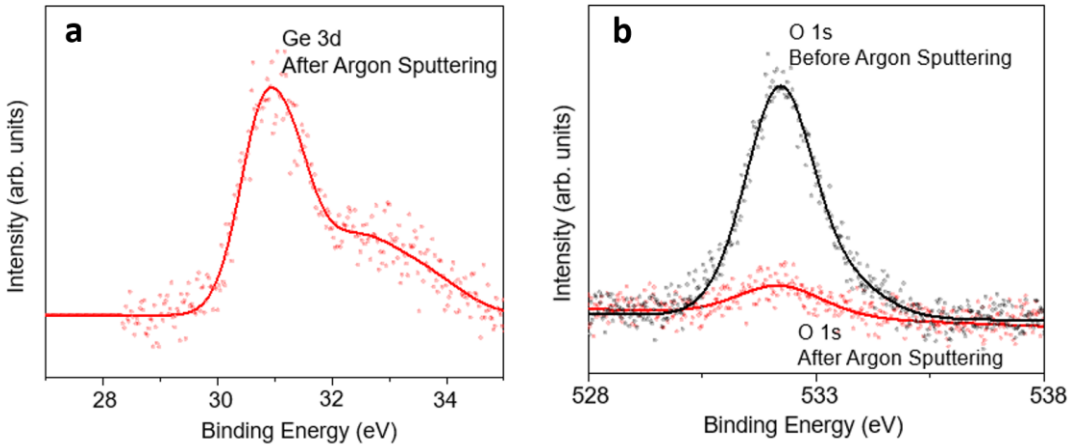


**Supplementary Figure 6. XPS characterization.** (a) XPS spectrum (Ge 3d) of $CsSn_{0.5}Ge_{0.5}I_3$ perovskite thin film (incidence angle: 15˚) after 15-s Ar-sputtering. (b) XPS spectra (O 1s) of $CsSn_{0.5}Ge_{0.5}I_3$ perovskite thin film (incidence angle: 15˚) before (black) and after (red) 15-s Ar-sputtering.

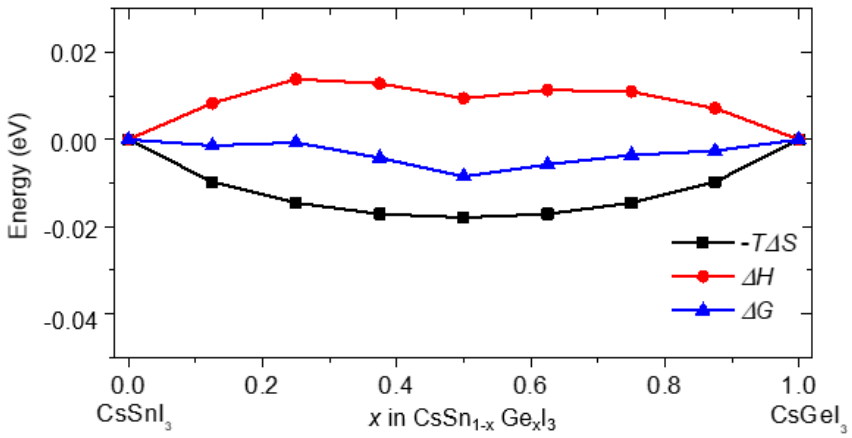


**Supplementary Figure 7. Energy calculations.** Calculated enthalpy, entropy, and Gibbs free energy at 300 K for $CsSn_{1-x}Ge_xI_3$ as a function of *x*. For simplicity, the $CsSn_{0.5}Ge_{0.5}I_3$ phase was assigned to have the space group of $\boldsymbol{R3m}$.

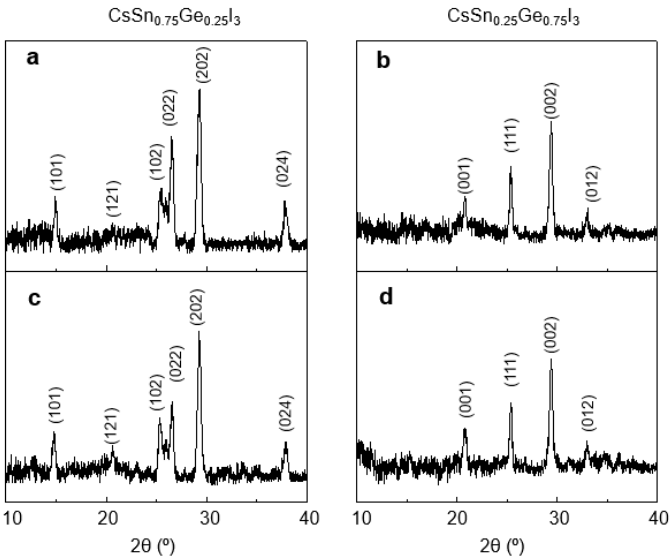


**Supplementary Figure 8. Relative stability of $CsSn_{0.75}Ge_{0.25}I_3$ and $CsSn_{0.25}Ge_{0.75}I_3$.** (a, b) XRD patterns of as-synthesized $CsSn_{0.75}Ge_{0.25}I_3$ and $CsSn_{0.25}Ge_{0.75}I_3$ powders, respectively. (c, d) XRD patterns of $CsSn_{0.75}Ge_{0.25}I_3$ and $CsSn_{0.25}Ge_{0.75}I_3$ powders after 24-h exposure to air (25 ˚C, 80% RH), respectively.

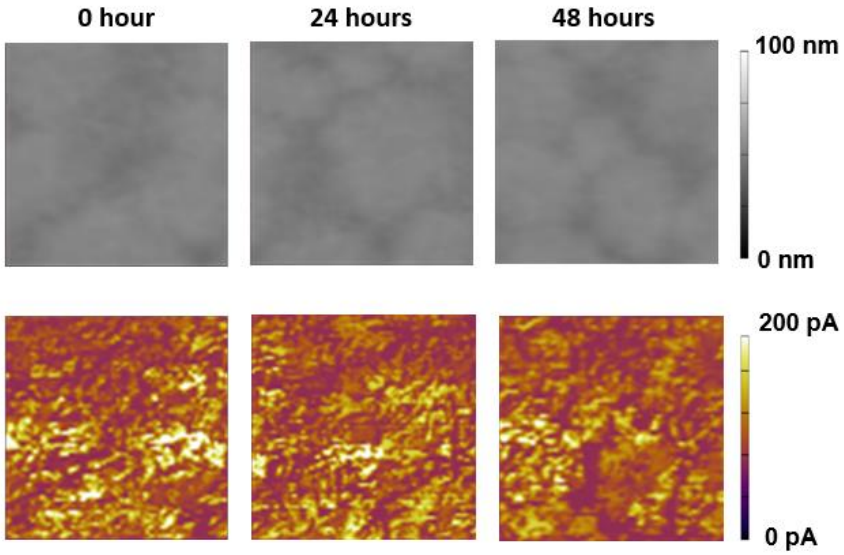


**Supplementary Figure 9. AFM and *c*-AFM mapping.** AFM topography (top) and corresponding *c*-AFM (bottom) maps over a 5×5-μm$^2$ area of the $CsSn_{0.5}Ge_{0.5}I_3$ perovskite thin film exposed to air for 0, 24 h, and 48 h.

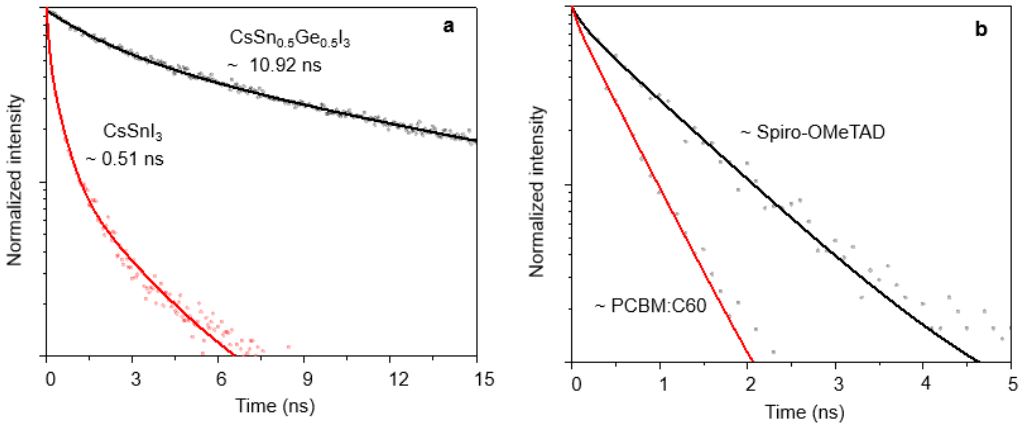


**Supplementary Figure 10. TRPL spectroscopy.** (a) TRPL results from the $CsSn_{0.5}Ge_{0.5}I_3$ and the $CsSnI_3$ perovskite thin film (thickness ~200 nm on glass substrates). (b) PL decay dynamics of the $CsSn_{0.5}Ge_{0.5}I_3$ perovskite thin films coated with an electron (PCBM:$C_{60}$) or a hole quenching (Spiro-OMeTAD) layer.

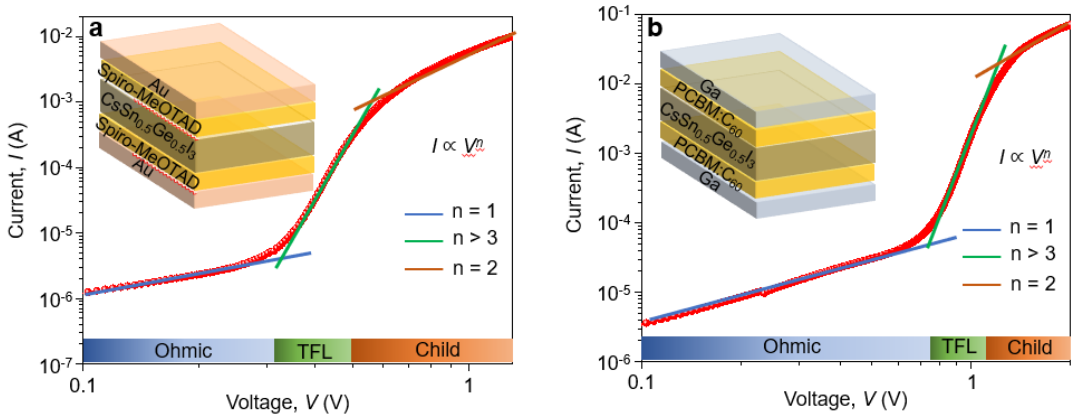


**Supplementary Figure 11. Film electrical properties.** *I-V* characteristics of $CsSn_{0.5}Ge_{0.5}I_3$ perovskite thin films for (a) hole-only transport (b) electron-only transport. Insets: the respective device architectures used.

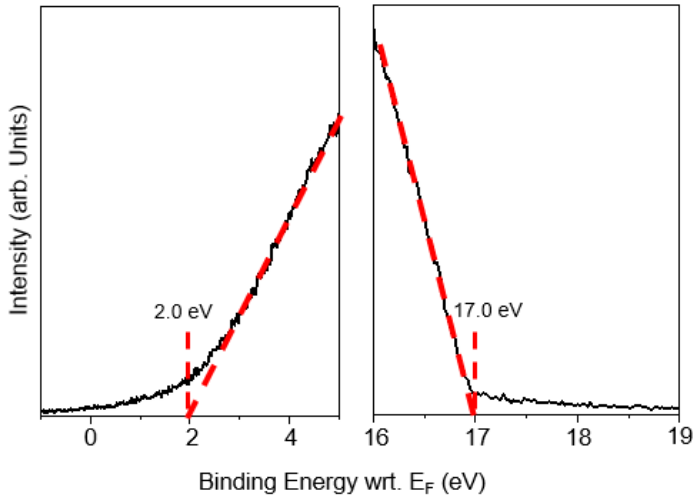


**Supplementary Figure 12. UPS characterization.** UPS data from the native oxide on the $CsSn_{0.5}Ge_{0.5}I_3$ perovskite thin film.

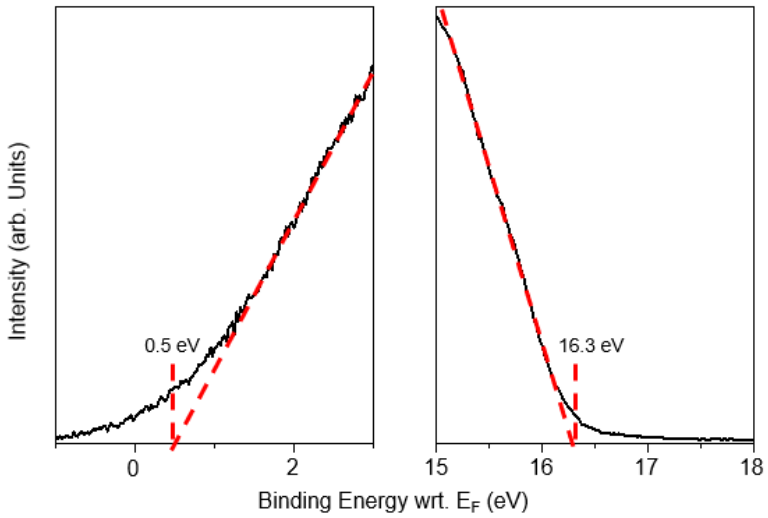


**Supplementary Figure 13. UPS characterization.** UPS data from the $CsSn_{0.5}Ge_{0.5}I_3$ perovskite thin film after 15-s Ar-sputtering.

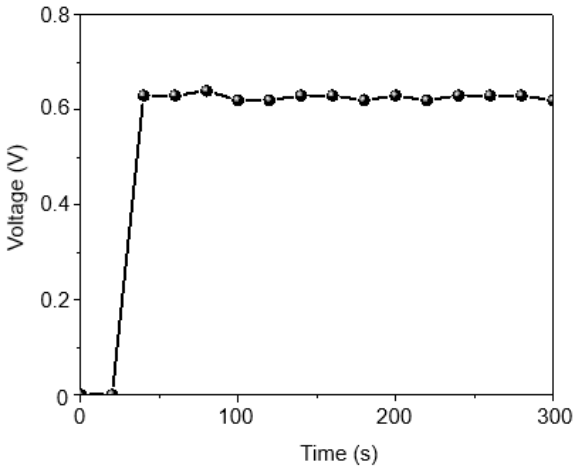


**Supplementary Figure 14. $V_{OC}$ stability.** The stability of the $V_{OC}$ of the PSC based on the $CsSn_{0.5}Ge_{0.5}I_3$ perovskite thin film. The $V_{OC}$ has been determined every other 20 seconds.

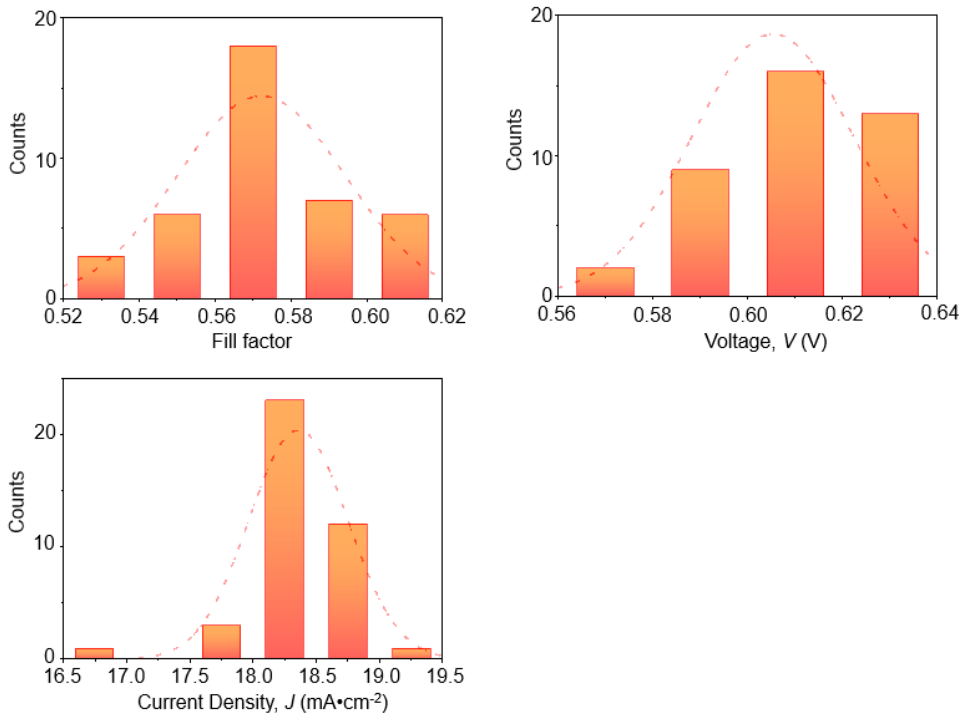


**Supplementary Figure 15. Performance statistics.** Detailed statistics of $J_{SC}$, $V_{OC}$ and FF from 40 $CsSn_{0.5}Ge_{0.5}I_3$-based PSCs.

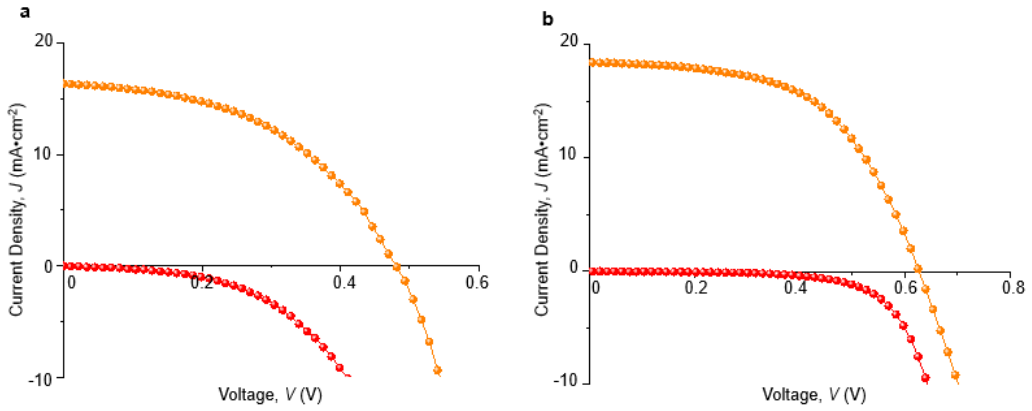


**Supplementary Figure 16. Performance of PSCs based on $CsSn_{0.5}Ge_{0.5}I_3$ perovskite thin films.** *J-V* responses (reverse scan) under 1-sun and in 'dark': (a) PSC without native oxide fabricated inside a $N_2$-filled glovebox ($O_2$ and $H_2O$ levels <0.1ppm) and (b) PSC with native oxide fabricated in ambient atmosphere.

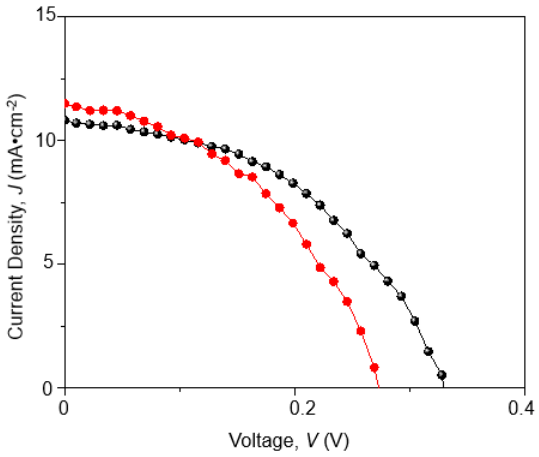


**Supplementary Figure 17. Performance of $CsSnI_3$-based PSCs.** *J-V* curves of $CsSnI_3$-based PSCs fabricated using the similar single-source evaporation method that is used for $CsSn_{0.5}Ge_{0.5}I_3$ in this work (red: forward scan, black: reverse scan).

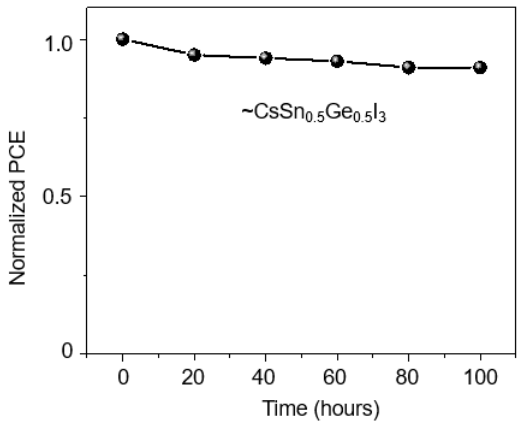


**Supplementary Figure 18. Air-stability.** PCE Stability of $CsSn_{0.5}Ge_{0.5}I_3$-based PSCs (unencapsulated) under continuous light illumination in the ambient air.

**Supplementary Table 1.** *J-V* parameters of the 40 PSC devices used for the statistics.

| Device No. | $V_{OC}$ (V) | FF | $J_{SC}$ (mA•cm$^{-2}$) | PCE (%) |
|---|---|---|---|---|
| 1 | 0.59 | 0.562 | 18.457 | 6.119 |
| 2 | 0.59 | 0.556 | 18.625 | 6.11 |
| 3 | 0.59 | 0.544 | 18.351 | 5.89 |
| 4 | 0.59 | 0.544 | 18.164 | 5.83 |
| 5 | 0.58 | 0.544 | 17.653 | 5.57 |
| 6 | 0.58 | 0.536 | 17.884 | 5.559 |
| 7 | 0.57 | 0.536 | 18.198 | 5.56 |
| 8 | 0.57 | 0.536 | 16.758 | 5.119 |
| 9 | 0.63 | 0.613 | 18.41 | 7.11 |
| 10 | 0.63 | 0.613 | 18.255 | 7.049 |
| 11 | 0.63 | 0.608 | 18.379 | 7.039 |
| 12 | 0.63 | 0.608 | 18.353 | 7.029 |
| 13 | 0.63 | 0.608 | 18.248 | 6.99 |
| 14 | 0.62 | 0.605 | 18.261 | 6.85 |
| 15 | 0.62 | 0.595 | 18.181 | 6.707 |
| 16 | 0.62 | 0.592 | 18.526 | 6.8 |
| 17 | 0.62 | 0.592 | 18.472 | 6.78 |
| 18 | 0.59 | 0.562 | 18.456 | 6.119 |
| 19 | 0.61 | 0.568 | 18.615 | 6.449 |
| 20 | 0.61 | 0.568 | 18.327 | 6.35 |
| 21 | 0.61 | 0.566 | 18.334 | 6.33 |
| 22 | 0.6 | 0.566 | 18.404 | 6.249 |
| 23 | 0.6 | 0.566 | 18.345 | 6.229 |
| 24 | 0.6 | 0.566 | 18.345 | 6.229 |
| 25 | 0.6 | 0.566 | 18.256 | 6.199 |
| 26 | 0.6 | 0.566 | 18.021 | 6.12 |
| 27 | 0.6 | 0.566 | 18.021 | 6.12 |
| 28 | 0.62 | 0.586 | 18.661 | 6.78 |
| 29 | 0.62 | 0.586 | 18.661 | 6.78 |
| 30 | 0.62 | 0.583 | 18.757 | 6.779 |
| 31 | 0.61 | 0.576 | 19.296 | 6.78 |
| 32 | 0.61 | 0.576 | 18.869 | 6.63 |
| 33 | 0.61 | 0.576 | 18.641 | 6.55 |
| 34 | 0.61 | 0.573 | 18.71 | 6.54 |
| 35 | 0.61 | 0.569 | 18.669 | 6.48 |
| 36 | 0.61 | 0.568 | 18.673 | 6.47 |
| 37 | 0.6 | 0.566 | 18.346 | 6.229 |
| 38 | 0.58 | 0.544 | 18.16 | 5.73 |
| 39 | 0.58 | 0.544 | 17.97 | 5.669 |
| 40 | 0.62 | 0.588 | 18.597 | 6.779 |